Invited Paper

Towards four-dimensional photonics

Hannah M. Price[a], Tomoki Ozawa[a], Nathan Goldman[b], Oded Zilberberg[c], and Iacopo Carusotto[a]

[a]INO-CNR BEC Center and Dipartimento di Fisica, Università di Trento, I-38123 Povo, Italy
[b]CENOLI, Faculté des Sciences, Université Libre de Bruxelles (U.L.B.), B-1050 Brussels, Belgium
[c]Institute for Theoretical Physics, ETH Zurich, 8093 Zürich, Switzerland

ABSTRACT

Recent advances in silicon ring-resonator arrays have stimulated the development of topological lattices for photons, with potential applications in integrated photonic devices. Taking inspiration from ultracold atoms, we propose how such arrays can be extended into an additional synthetic dimension by coupling together the different modes of each ring resonator.[1] In this way, a 1D resonator chain can become an effective 2D system, while a 3D resonator array can be exploited as a 4D photonic lattice. As an example of the power of this approach, we discuss how to experimentally realise an optical analogue of the 4D quantum Hall effect for the first time. This opens up the way towards the exploration of higher-dimensional lattices in integrated photonics.

Keywords: synthetic dimensions, quantum Hall effect, topological physics, synthetic gauge fields, coupled ring resonators, higher-dimensional photonic lattices

1. INTRODUCTION

Topological physics has emerged over the last decades as a unifying concept, bringing together advances in solid-state physics,[2–4] ultracold gases,[5–7] mechanical systems[8–10] and photonics.[11–19] In these systems, quantum-mechanical or classical waves can propagate through periodic structures, setting up modes that form energy bands when plotted as a function of energy versus quasimomentum. It was long thought that all important physical information, in the absence of interparticle interactions, could be extracted directly from these plots, such as, e.g. the group velocity which is found by taking the gradient of a band with respect to the quasimomentum. A key realisation was that in fact the modes of an energy band can also have important geometrical and topological properties. Energy bands characterised by nontrivial topological invariants, for example, are associated with robust edge physics and quantized bulk responses[3,4] such as the archetypical 2D quantum Hall effect.[2]

While topological physics originated with electrons in solid-state materials, the control and design flexibility that is rapidly becoming possible in engineered bosonic systems of photons or ultracold atoms has opened up many new avenues of topological research. Since the first proposal for topological photonics in 2008,[12] there have been experimental explorations of topological physics in gyromagnetic photonic crystals for microwaves,[13] in coupled optical waveguides,[15,16] in metamaterials[20] and in arrays of silicon micro-ring resonators.[14] In particular, the last of these experiments has raised the intriguing possibility of using topological properties to design novel components for on-chip optical circuits, such as robust optical delay lines.[21] The current interest in engineering topological models in integrated photonics has therefore been sparked both by the hope of practical applications as well as the opportunity to explore new types of topological phenomena.

An important tool that will allow integrated photonics to go beyond what is possible for solid-state materials is the introduction of a so-called "synthetic" dimension. While this concept was first proposed[22,23] and experimentally realised in ultracold atoms,[24,25] it has since been theoretically extended to various optical systems.[1,18,19,26] In integrated photonics, in particular, we have recently proposed how the different modes of a silicon micro-ring resonator could be re-interpreted as the sites along a synthetic dimension.[1] By coupling together different modes, photons can "hop" between modes, just like particles can tunnel between lattice sites. In this way, photons in an array of ring resonators in d_{real} spatial dimensions behave as if they explore a system with $d_{\mathrm{real}}+1$ dimensions. This means that a 1D chain of resonators can act like an effective 2D system, or

Advances in Photonics of Quantum Computing, Memory, and Communication IX, edited by Zameer Ul Hasan, Philip R. Hemmer, Hwang Lee, Alan L. Migdall, Proc. of SPIE Vol. 9762, 97620V
 · doi: 10.1117/12.2218539

that a 3D array of resonators could behave like a 4D lattice. While topological physics in higher dimensions, such as the 4D quantum Hall effect, have been theoretically studied,[27,28] this physics was long expected to be inaccessible directly in experiments. Now with a synthetic dimension, these effects may be within experimental reach.[29]

In these proceedings, we begin in Section 2 by reviewing how a synthetic dimension can be introduced for silicon micro-ring resonators.[1] Then in Section 3 we introduce the 4D quantum Hall effect, which we will use as a case-study to demonstrate how synthetic dimensions can be used to push beyond the current state-of-the-art. In Section 4, we expand upon our recent proposal for realising an optical analogue of the 4D quantum Hall effect with a 3D ring resonator array,[1] providing additional details and calculations aimed at future experiments. Finally in Section 5, we present our conclusions.

2. SYNTHETIC DIMENSION FOR RING RESONATOR LATTICES

Light resonates in a silicon micro-ring whenever it constructively interferes with itself after a full round-trip around the cavity.[30] Each of these so-called "whispering gallery" modes can be labelled by an index w, corresponding to the orbital angular momentum of the mode around the ring. As we introduce in Section 2.1, this mode index w can be reinterpreted as a site index along an additional synthetic dimension on a single ring resonator. In Section 2.2, we review how this formalism extends an array of ring resonators in d_{real} spatial dimensions to an effective system of $d_{\text{real}}+1$ dimensions, including the synthetic dimension.

2.1 Synthetic dimension for a single ring resonator

Usually, the different whispering gallery modes of a ring-resonator are uncoupled and photons remain in the same w mode until they are lost from the cavity. To reinterpret these modes instead as a synthetic dimension, photons should be able to change modes and so move along the synthetic dimension. As we have recently proposed,[1] an appropriate inter-mode coupling could be implemented via an external time-dependent modulation of the dielectric properties of a ring resonator. For example, this can be achieved by applying strong external light fields to a ring resonator, and so generating a significant modulation of the susceptibility tensor through either the $\chi^{(2)}$ or $\chi^{(3)}$ nonlinearities of the material. In a closely-related scheme, that has since been put forward, the required dielectric modulation can be introduced by placing an electro-optic modulator at a single point on the ring resonator.[26] A similar idea for coupling different angular momentum states of coupled resonator loops has also previously been realised.[31]

The time-dependent modulation of the dielectric properties leads to an effective Hamiltonian:[1]

$$H_{\text{mod}} = -\sum_{w} \mathcal{J}_{\mathbf{r}}(t)\, \hat{a}^{\dagger}_{\mathbf{r},w+\eta} \hat{a}_{\mathbf{r},w} + \text{h.c.}, \tag{1}$$

(taking $\hbar = 1$), where $\mathcal{J}_{\mathbf{r}}(t)$ is the inter-mode coupling amplitude which is determined by the details of the modulation scheme. Here, the index $\mathbf{r} = (x, y, z)$ labels the spatial position of the resonator, while $\hat{a}^{\dagger}_{\mathbf{r},w}$ creates a photon in the resonator mode w. The hopping unit η corresponds to how many units of angular momentum are transferred to the photon in the coupling process; in Figure 1, for example, the inter-mode coupling is depicted between adjacent modes, corresponding to $\eta = 1$. This Hamiltonian is similar to that describing a particle hopping along a tight-binding chain of lattice sites, although the hopping amplitude varies in time.

To go further, we can exploit the fact that whispering gallery modes are almost equispaced in frequency by the free spectral range $\Delta\Omega = 2\pi c/(n_{\text{eff}} R)$, where R is the ring radius and n_{eff} is the effective refractive index. We write the mode spectrum as[1]

$$\Omega_w = \Omega_{w_0} + \Delta\Omega\,(|w| - w_0) + \frac{D}{2}(|w| - w_0)^2 + \ldots, \tag{2}$$

where the frequency dispersion D is due to the confinement geometry and to the residual refractive index dispersion of the material. The contribution of the dispersion is typically small if one works with the reference mode $w_0 \gg 1$. This spectrum is sketched schematically in Figure 1. We can therefore choose the modulation to be monochromatic with $\mathcal{J}_{\mathbf{r}}(t) = \mathcal{J}^{o}_{\mathbf{r}} e^{-i\Omega_{\text{mod}} t}$, as a single, suitable coupling frequency $\Omega_{\text{mod}} \approx \eta\Delta\Omega$ simultaneously

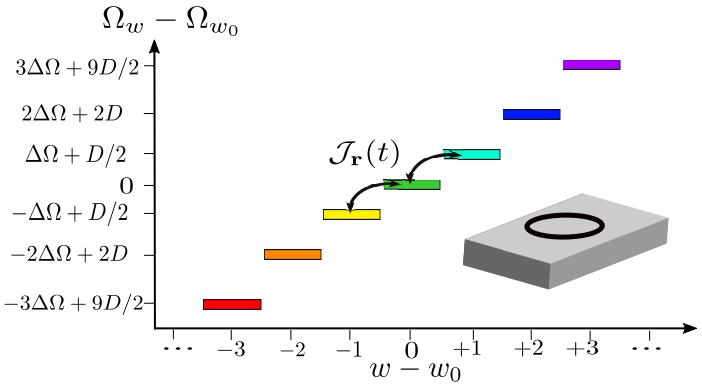

Figure 1. The discrete whispering gallery modes of a single micro-ring resonator can be reinterpreted as an additional synthetic dimension, along which sites are labelled by the angular momentum w. The frequencies of these modes (2) are indicated for a small window around a reference mode with w_0. Close to this mode, the mode frequencies are approximately equally spaced by the free spectral range $\Delta\Omega$, with a small correction due to the dispersion D. Photons can "hop" between different resonator modes thanks to an external modulation of the dielectric properties of the cavity. The associated transitions for the w_0 mode are highlighted here for a monochromatic modulation at frequency $\Omega_{\text{mod}} \approx \Delta\Omega$, with $\eta = 1$.

couples many pairs of states.[1] For this simple choice of modulation, we move to a rotating frame by the transformation

$$\hat{b}_{\mathbf{r},w}(t) \equiv \hat{a}_{\mathbf{r},w}(t) e^{i[\Omega_{w_0} + (w-w_0)\Omega_{\text{mod}}/\eta]t}, \tag{3}$$

which we apply to the full Hamiltonian of the modulated ring-resonator: $H = H_{\text{mod}} + \sum_{w,\mathbf{r}} \Omega_w \hat{a}^\dagger_{\mathbf{r},w} \hat{a}_{\mathbf{r},w}$. Then we arrive finally at the time-independent Hamiltonian[1]

$$H_\Omega = \sum_w \left[-\mathcal{J}^o_{\mathbf{r}} \hat{b}^\dagger_{\mathbf{r},w+\eta} \hat{b}_{\mathbf{r},w} + \text{h.c.} + \left((\Delta\Omega - \Omega_{\text{mod}}/\eta)(w - w_0) + \frac{D}{2}(w - w_0)^2 \right) \hat{b}^\dagger_{\mathbf{r},w} \hat{b}_{\mathbf{r},w} \right], \tag{4}$$

where we have focused around $w \approx w_0$. In this Hamiltonian, the first two terms again correspond to hopping along the synthetic dimension, but now with a time-independent hopping amplitude. The hopping amplitude, $\mathcal{J}^o_{\mathbf{r}} = |\mathcal{J}^o_{\mathbf{r}}| \exp[i\theta(\mathbf{r})]$, may also be made spatially-dependent and complex-valued. This is a valuable tool as the hopping phase-factor $\exp[i\theta(\mathbf{r})]$ mimics the Peierls phase-factor gained by a charged particle hopping in a lattice in the presence of a magnetic vector potential. As we shall discuss further below, this can be extended for an array of resonators to straightforwardly simulate artificial magnetic fluxes for photons, and so to realise topological physics in integrated photonics.[1] The third and fourth terms in this Hamiltonian are instead analogous respectively to a force and a harmonic trap along the w direction; however, for the purposes of this work, we neglect these terms by assuming that the detuning $(\Delta\Omega - \Omega_{\text{mod}}/\eta)$ and the dispersion D are negligible for the modes considered.

2.2 Synthetic dimension for an array of ring resonators

In an array of ring resonators, the spatial overlap of optical modes between neighbouring rings means that photons can also evanescently tunnel between the resonators. This can be described by the tight-binding Hamiltonian[1]

$$H_J = -\sum_{\mathbf{r},j,w} J_j \, \hat{b}^\dagger_{\mathbf{r}+a\mathbf{e}_j,w} \hat{b}_{\mathbf{r},w} + \text{h.c.}, \tag{5}$$

where the sum over $\mathbf{r}$ is over all resonator positions, where $\mathbf{e}_j$ is the unit vector between resonators in the real-space j direction, and we assume a is the lattice spacing along all directions. In this work, we focus on a 3D array of resonators, as shown in Figure 2, for which $j \in \{x, y, z\}$. The hopping amplitudes J_j drop off quickly with the inter-resonator distance due to the decreasing overlap of optical modes; this rapid drop-off justifies the inclusion of only nearest-neighbour hopping terms in our tight-binding model.

When the inter-mode coupling introduced above is also imposed, the total Hamiltonian is given by $H_{tot} = H_J + \sum_{\mathbf{r}} H_\Omega$ in the rotating frame. This means that photons behave as if they explore a system with an extra spatial dimension. For example, photons in a 1D chain of ring resonators experience an effective 2D lattice; this may have practical applications in building on-chip optical isolators[1] or in the high-efficiency generation of high-order side-bands.[26] Going further still, photons in a 3D array of ring resonators can simulate an effective 4D lattice.[1] As we discuss for the remainder of this work, in this way, a synthetic dimension in a ring resonator array could be exploited for the first experimental exploration of the 4D quantum Hall effect.

3. INTRODUCTION TO THE 4D QUANTUM HALL EFFECT

The 4D quantum Hall effect is a higher-dimensional cousin of the well-known 2D quantum Hall effect that ignited the field of topological phases of matter in the 1980s.[2] We briefly review this original 2D quantum Hall effect in Section 3.1, before highlighting the key characteristics of the more unfamiliar 4D effect in Section 3.2. Then in Section 3.3, we introduce our recently-proposed minimal lattice model for realising the 4D quantum Hall effect.[1]

3.1 The 2D quantum Hall effect

In the 2D quantum Hall effect, the current density of a filled isolated band of electrons is precisely quantised under the application of an external electric field, e.g. $\mathbf{E} = E_y \mathbf{e}^y$, as:

$$j^x = -eE_y \nu_1, \tag{6}$$

where e is the charge of the electron and ν_1 is the so-called first Chern number. The first Chern number is a topological invariant of the filled energy band[2] defined as:

$$\nu_1 \equiv \frac{1}{2\pi} \int_{\mathrm{BZ}} \mathcal{F}^{xy} d^2k \ \in \mathbb{Z}, \tag{7}$$

where the integral over the Brillouin zone (BZ) is of the geometrical Berry curvature $\mathcal{F}^{xy}$,

$$\mathcal{F}^{xy} \equiv i \left[\left\langle \frac{\partial u}{\partial k_x} \middle| \frac{\partial u}{\partial k_y} \right\rangle - \left\langle \frac{\partial u}{\partial k_y} \middle| \frac{\partial u}{\partial k_x} \right\rangle \right], \tag{8}$$

and $|u(\mathbf{k})\rangle$ are the Bloch states of the energy band. As a topological integer, the first Chern number cannot be changed by small perturbations, or more precisely, it stays constant as long as the energy band gap remains open. Consequently, the 2D quantum Hall effect is remarkably robust against both disorder and fabrication imperfections. For a system of charged particles, a practical way to engineer a band with a non-zero first Chern number is to apply a magnetic flux. However, for neutral particles, such as photons, other physical mechanisms can be used as will be introduced below.

3.2 The 4D quantum Hall effect

In 4D, a new type of quantised current response has been proposed which depends on both a perturbing magnetic field as well as an electric field.[27,28] This perturbing magnetic field can be expressed as $\delta B_{\rho\sigma} \equiv \partial_\rho A_\sigma - \partial_\sigma A_\rho$, where $\mathbf{A}$ is the perturbing magnetic vector potential in four spatial dimensions and where indices now run over all four dimensions $\rho, \sigma \in \{x, y, z, w\}$. The current density for a filled energy band is:[29]

$$j^\mu = -eE_\nu \int_{\mathrm{BZ}} \frac{d^4k}{(2\pi)^4} \mathcal{F}^{\mu\nu}(\mathbf{k}) + e^2 E_\nu \delta B_{\rho\sigma} \frac{\nu_2}{(2\pi)^2} \epsilon^{\mu\nu\rho\sigma}, \tag{9}$$

with $\epsilon^{\mu\nu\rho\sigma}$ being the 4D Levi-Civita symbol and with the integral taken over the full 4D Brillouin zone. While the first term here is closely related to the usual 2D quantum Hall response (6), the second term can only appear in four or higher dimension. Most importantly, this term depends on an integer ν_2, which is the so-called second Chern number (2CN): a 4D topological invariant of the energy band. In this work, we focus on a non-degenerate energy band for which the second Chern number can be written as

$$\nu_2 \equiv \frac{1}{(2\pi)^2} \int_{\mathrm{BZ}} \left(\mathcal{F}^{xy}\mathcal{F}^{zw} + \mathcal{F}^{wx}\mathcal{F}^{zy} + \mathcal{F}^{zx}\mathcal{F}^{yw} \right) d^4k \ \in \mathbb{Z}, \tag{10}$$

where the Berry curvature components are defined as in Eq. (8) for each 2D plane. To realise the 4D quantum Hall effect experimentally therefore requires (i) the realisation of a 4D lattice with a non-zero topological second Chern number and (ii) the creation and control of perturbing "electric" and "magnetic" fields appearing in Eq. (9). For the first of these ingredients, we now introduce an appropriate minimal lattice model, on which to base the experimental proposal that we recently proposed[1] and outlined here in greater detail in Section 4.

3.3 A minimal 4D lattice model for the 4D quantum Hall effect

To design a minimal system exhibiting the 4D quantum Hall effect, a natural starting place is the definition of the second Chern number in Eq. (10). This suggests that an appropriate lattice model is one with nontrivial Berry curvature in at least two disconnected planes, for example, the $x-w$ and $y-z$ planes. A particularly simple case is one in which the only non-zero Berry curvatures are of the form[29,32]

$$\mathcal{F}^{wx}(k_x,k_w)=-\mathcal{F}^{xw}(k_x,k_w)\neq 0,\quad \mathcal{F}^{zy}(k_y,k_z)=-\mathcal{F}^{yz}(k_y,k_z)\neq 0, \tag{11}$$

so that the 2CN (10) is directly $\nu_2=\nu_1^{xw}\times\nu_1^{yz}$, where we have introduced the first Chern numbers (7) associated with the $x-w$ and $y-z$ planes respectively. There are many known 2D models with nonzero first Chern numbers, and so a straightforward approach is to combine any two such models, one in each disconnected plane, to create a composite 4D model. One of the simplest choices for the 2D model is the Harper-Hofstadter (HH) model[33] of a charged particle hopping on a 2D square lattice in a uniform magnetic flux, i.e., it is the lattice version of the 2D Hall effect discussed in Section 3.1. The resulting minimal 4D model, consisting of a copy of the HH model in each of the two planes, is given in the Landau gauge by:[1,29,32]

$$\hat{H}=-J\sum_{\boldsymbol{r},w} b^\dagger_{\boldsymbol{r}+a\boldsymbol{e}_x,w}b_{\boldsymbol{r},w}+b^\dagger_{\boldsymbol{r}+a\boldsymbol{e}_z,w}b_{\boldsymbol{r},w}+e^{i2\pi\Phi_{yz}z/a}b^\dagger_{\boldsymbol{r}+a\boldsymbol{e}_y,w}b_{\boldsymbol{r},w}+e^{i2\pi\Phi_{xw}x/a}b^\dagger_{\boldsymbol{r},w+\eta}b_{\boldsymbol{r},w}+\text{h.c.}, \tag{12}$$

where we have set the real part of the hopping amplitudes along the physical and the synthetic dimensions all equal to J. Here, Φ_{xw} and Φ_{yz} are the uniform magnetic fluxes piercing the $x-w$ and $y-z$ planes respectively. In what follows, we assume the fluxes are rational, i.e. that they can be expressed as $\Phi_{\mu\nu}=q_{\mu\nu}/p_{\mu\nu}$ where $q_{\mu\nu}$ and $p_{\mu\nu}$ are co-prime integers, and that they lead to isolated non-degenerate bands. Deviations from this simple case will be presented elsewhere.[34] Then, as has been numerically verified,[29] this 4D model has all the key characteristics required to explore the 4D quantum Hall effect described above: for suitable choices of the fluxes, it has a lowest energy band which is well-isolated, non-degenerate and has a non-zero second Chern number. Most importantly, as we now discuss, this model could also be within experimental reach in integrated photonics.

4. 4D QUANTUM HALL PHYSICS IN A 3D ARRAY OF RING RESONATORS

We propose to exploit a 3D array of resonators with a synthetic dimension to study the 4D quantum Hall effect. In Section. 4.4 and Section. 4.2, we detail how the necessary ingredients can be realised in integrated photonics. We then discuss in Section 4.3 how the 4D quantum Hall effect could be probed in a driven-dissipative optical system, before presenting numerical simulations and discussion of possible experiments in Section 4.4.

4.1 The minimal 4D topological lattice model in photonics

We consider a 3D array of ring resonators extended into an effective 4D system by a synthetic dimension, sketched in Figure 2(a). As we outlined in Sec. 2, this system can be described by a tight-binding Hamiltonian $H_{tot}=H_J+\sum_{\mathbf{r}}H_\Omega$, including hopping terms along all four dimensions. Compared with the minimal topological lattice model in Eq. (12), the key extra ingredient required is the modification of certain hopping processes by complex spatially-dependent phase factors, to mimic the effects of magnetic fluxes on charged particles. As the physical mechanism for imposing such phase factors is different in the synthetic versus the spatial dimensions, we consider these separately in turn.

1.Synthetic flux in the y-z plane– Along real spatial directions, appropriate hopping phases can be created by introducing off-resonant *link resonators*, as in the recent experiment for a 2D array of ring resonators.[14] By displacing the link resonators along the y direction by an amount α that depends on the position along z, as shown in Figure 2(b), light gains a net phase-shift as it travels around a plaquette in the $y-z$ plane equal

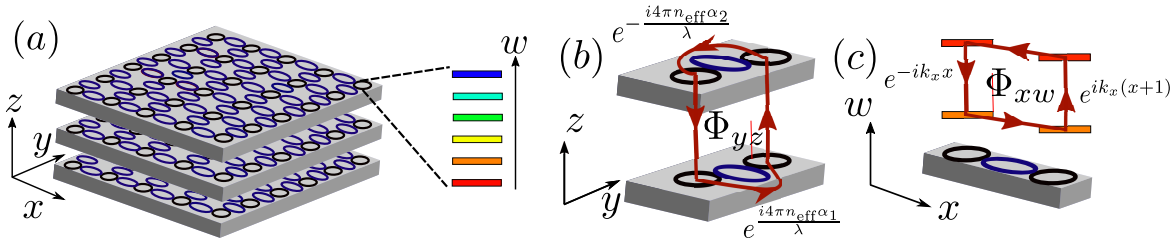

Figure 2. (a) The proposed 4D photonic lattice consisting of a 3D ring-resonator array combined with a synthetic dimension $\hat{w}$ provided by the different whispering gallery modes of each resonator. The resonant microrings (in black) are the spatial lattice sites labelled by $\mathbf{r}$, while the off-resonant microrings (in blue) are used to implement synthetic gauge fields in the real spatial dimensions.[14] This is shown schematically in (b) for a plaquette in the $y-z$ plane. Photons travelling around a single plaquette gain a complex phase from the z-dependent displacement of the off-resonant rings along y. This can be seen as imposing a synthetic flux Φ_{yz} on the photons.[14] (c) A plaquette in the $x-w$ plane in which the synthetic flux Φ_{xw} can be realised by choosing the external modulation coupling different modes to have a spatial dependence as $\mathcal{J}^o_{\mathbf{r}} = |\mathcal{J}^o_{\mathbf{r}}|e^{ik_x x}$. Combining the synthetic fluxes in (b) and (c) leads to a topological lattice model that can exhibit the 4D quantum Hall effect.[1,29]

to $\Phi_{yz} = 4\pi n_{\text{eff}}\Delta\alpha/\lambda$, where $\Delta\alpha = \alpha_1 - \alpha_2$ is the difference in the displacement of the two link resonators and λ is the wavelength of the light considered.[14] The hopping phase does depend on w via λ, however, we assume this dependence is weak over the frequencies considered and can be ignored. We note that the insertion of link resonators does not break time-reversal symmetry, unlike a true magnetic field for a charged electron. Instead, photons with positive angular momentum w can in principle backscatter into states with negative angular momentum $-w$ through impurities. Photons in the modes with negative angular momentum will hop under an opposite magnetic flux $-\Phi_{yz}$. We assume that such a backscattering can, however, be minimised in fabrication as in the previous 2D experiment.[14] Finally, we note that as the hopping along z is via evanescent coupling rather than link resonators, care must be taken in the experimental design to ensure that the hopping amplitudes J_j are indeed all equal.

2. Synthetic flux in the x-w plane– As introduced briefly above, the amplitude $\mathcal{J}^o_{\mathbf{r}}$ of the dielectric tensor modulation, which controls the hopping along w, can be made complex and spatially-dependent. For example, we choose the modulation amplitude as $\mathcal{J}^o_{\mathbf{r}} = |\mathcal{J}^o_{\mathbf{r}}|e^{ik_x x}$, then, as indicated in Figure 2(c), the hopping around a plaquette in the $x-w$ plane encloses a "magnetic flux" of $\Phi_{xw} = k_x a/2\pi$. The strength of the artificial magnetic flux can therefore be tuned through the wave-vector k_x of the dielectric modulation, which can in turn be controlled, for example, via optical fields inducing this modulation through material nonlinearities.[1] We note that, unlike above, the modulation can break time-reversal symmetry, and so be robust against backscattering. Together, the combination of these two methods can be used to realise the 4D topological lattice model of Eq. (12) and generate photonic energy bands with non-zero 2CNs.

4.2 Perturbing "electric" and "magnetic" fields in photonics

The second key ingredient required for 4D quantum Hall physics is the creation and control of the perturbing electric and magnetic fields in Eq. (9). Experimentally, the simplest way to implement a perturbing magnetic field is to give the modulation amplitude an additional spatial dependence, for example, $\mathcal{J}^o_{\mathbf{r}} = |\mathcal{J}^o_{\mathbf{r}}|e^{ik_x x}e^{ik_z z}$. By the same argument as above, this leads to a perturbing magnetic flux of $\delta\Phi_{zw} = k_z a/2\pi$. Provided that $k_z \ll k_x$, the artificial magnetic flux satisfies $|\delta\Phi_{zw}| \ll |\Phi_{xw}|$, and so the former can be treated as a perturbation To connect with Eq. (9), the artificial flux can be expressed as a perturbing artificial magnetic field, δB_{zw}, through $\delta\Phi_{zw} = \eta a e \delta B_{zw}/2\pi$, where e is the fictitious "charge" and (ηa) is the "area" of a plaquette in the $z-w$ plane.

From Eq. (9), we see that only certain combinations of electric and magnetic fields will lead to the interesting nonlinear 4D topological response, due to the 4D Levi-Civita symbol. For a perturbing magnetic field δB_{zw}, the appropriate electric field would be E_x or E_y; electric fields along w or z will only lead to linear 2D-like responses. Experimentally, electric fields along real spatial directions such as x or y can be created by varying either the cavity size or the temperature uniformly in space; hereafter, we assume that $\mathbf{E} = E_x \boldsymbol{e}^x$.

4.3 Driven-dissipative optical analogue of the 4D quantum Hall effect

Light in an array of silicon ring resonators is an inherently driven-dissipative system, while the quantized quantum Hall current responses [Eq. (6) & Eq. (9)] are derived considering conservative dynamics. However, as we briefly review, clear analogues of quantum Hall effects may still be found even with the pumping and losses in photonic systems.[1,35] Theoretically, our system can be modelled by assuming that light leaks out of the resonators with a position- and mode-dependent loss rate $\gamma_{\mathbf{r},w}$, while a "probe beam" pumps the system continuously. We assume that this probe beam is sufficiently weak that we can neglect photon-photon interactions. Then, the expectation value of the cavity field $\beta_{\mathbf{r},w}(t) \equiv \langle \hat{b}_{\mathbf{r},w}(t) \rangle$ in our effective 4D system (12) evolves according to:[35]

$$\begin{aligned} i\frac{\partial}{\partial t}\beta_{\mathbf{r},w} = &- J[\beta_{\mathbf{r}-a\boldsymbol{e}_x,w} + \beta_{\mathbf{r}+a\boldsymbol{e}_x,w} + \beta_{\mathbf{r}-a\boldsymbol{e}_z,w} + \beta_{\mathbf{r}+a\boldsymbol{e}_z,w} + e^{i2\pi\Phi_{yz}z/a}\beta_{\mathbf{r}-a\boldsymbol{e}_y,w} + e^{-i2\pi\Phi_{yz}z/a}\beta_{\mathbf{r}+a\boldsymbol{e}_y,w}] \\ &+ e^{i2\pi(\Phi_{xw}x+\delta\Phi_{zw}z)/a}\beta_{\mathbf{r},w-\eta} + e^{-i2\pi(\Phi_{xw}x+\delta\Phi_{zw}z)/a}\beta_{\mathbf{r},w+\eta}] + [-i\gamma_{\mathbf{r},w} + eE_x x]\beta_{\mathbf{r},w} + f_{\mathbf{r},w}(t), \end{aligned} \tag{13}$$

where the hopping amplitudes are assumed to be equal $J_j = |\mathcal{J}^o_{\mathbf{r}}| = J$ and where $f_{\mathbf{r},w}(t)$ is the probe beam as seen in the rotating frame. We assume that the probe is only applied to a single ring at position $\mathbf{r}$, and that it is monochromatic $f_{\mathbf{r},w}(t) \propto e^{-i\Omega_{\text{drive}}t}$ at a driving frequency Ω_{drive}. This corresponds in the non-rotating frame to a frequency $\Omega_w + \Omega_{\text{drive}}$. Provided that $\Omega_{\text{drive}} \ll \Delta\Omega$, only one mode w of one resonator $\mathbf{r}$, is effectively driven. After a sufficiently long time, the photons in the system reach a steady-state distribution; this can be found numerically by solving the above equation of motion over a finite 4D lattice.

The optical analogue of the 4D quantum Hall effect [Eq. (9)] is observable as a displacement of the center-of-mass of the photon steady-state, e.g. $\langle y \rangle = [\sum_{\mathbf{r},w} y|\beta_{\mathbf{r},w}|^2]/[\sum_{\mathbf{r},w}|\beta_{\mathbf{r},w}|^2]$, when the probe beam excites all the states in an isolated band.[1,35] As we only pump a single resonator mode $(\mathbf{r}, w)$, we uniformly excite states at all quasimomenta in the Brillouin zone. To restrict this excitation then to states only within a single band, we choose Ω_{drive} to be on resonance with that band and ensure the loss rate satisfies $\Delta\mathcal{E}_{\text{band}} < \gamma < \Delta\mathcal{E}_{\text{gap}}$, for a band with bandwidth $\Delta\mathcal{E}_{\text{band}}$ and an energy gap to adjacent bands of $\Delta\mathcal{E}_{\text{gap}}$. Then it can be shown that:[1]

$$\begin{aligned} \langle w \rangle &= e\frac{(\eta a)q_{xw}}{\gamma}\frac{\nu_1^{xw}}{2\pi}E_x + \mathcal{O}(\gamma^0), \\ \langle y \rangle &= -e^2\frac{(\eta a^3)q_{yz}q_{xw}}{\gamma}\frac{\nu_2}{(2\pi)^2}E_x\delta B_{zw} + \mathcal{O}(\gamma^0) = -e\frac{a^2 q_{yz}q_{xw}}{\gamma}\frac{\nu_2}{2\pi}E_x\delta\Phi_{zw} + \mathcal{O}(\gamma^0). \end{aligned} \tag{14}$$

The response $\langle w \rangle$ is directly analogous to the first term in Eq. (9) as it also is linear in the applied perturbing fields and depends only on a 2D topological invariant ν_1^{xw}; we therefore refer to this below as the 2D-like quantum Hall response. The second response $\langle y \rangle$ is nonlinear, as it contains both E_x and $\delta\Phi_{zw}$, and it also depends on the 4D topological invariant ν_2; we refer to this as the 4D quantum Hall response.

4.4 Numerical simulations of the optical analogue of the 4D quantum Hall effect

To demonstrate these two effects, we numerically simulate the photon steady-state of a 4D lattice with uniform, non-perturbing fluxes $\Phi_{yz} = \Phi_{xw} = 1/8$, for which the lowest band has a second Chern number $\nu_2 = 1$ and $\nu^{yz} = \nu^{xw} = -1$. The resulting steady-state is shown in Figure 3 projected onto either the $x-y$ or $x-w$ plane for various combinations of the weak perturbing fields. As can be seen in Fig. 3(a)-(d), only in the presence of both perturbations, E_x and $\delta\Phi_{zw}$, is there a clear displacement along y; this is the analogue of the 4D quantum Hall response as expected from Eq. (14). Conversely, as can be seen in Fig. 3(e)-(h), the large displacement along w depends instead only on the presence of the electric field. This is the 2D-like quantum Hall effect in Eq. (14). We note that there is also a displacement along x in the presence of the artificial electric field [as can be seen in panels (b), (d), (f) & (h)]; this is the longitudinal response of the driven-dissipative photonic system to an external force, which has no analogue in the quantum Hall current of a filled band of electrons.[35]

We can also quantitatively extract the second Chern number from the numerical displacement of the photon steady-state $\langle y \rangle$ by using Eq. (14). This is demonstrated in Figure 4 where the extracted ν_2 is plotted as a function of the loss-rate γ for a 4D lattice with (A) $\Phi_{yz} = \Phi_{xw} = 1/8$ and (B) $\Phi_{xw} = 1/9, \Phi_{yz} = 6/13$, which have lowest bands with $\nu_2 = 1$ and $\nu_2 = -2$ respectively. In this figure, the second Chern number is extracted

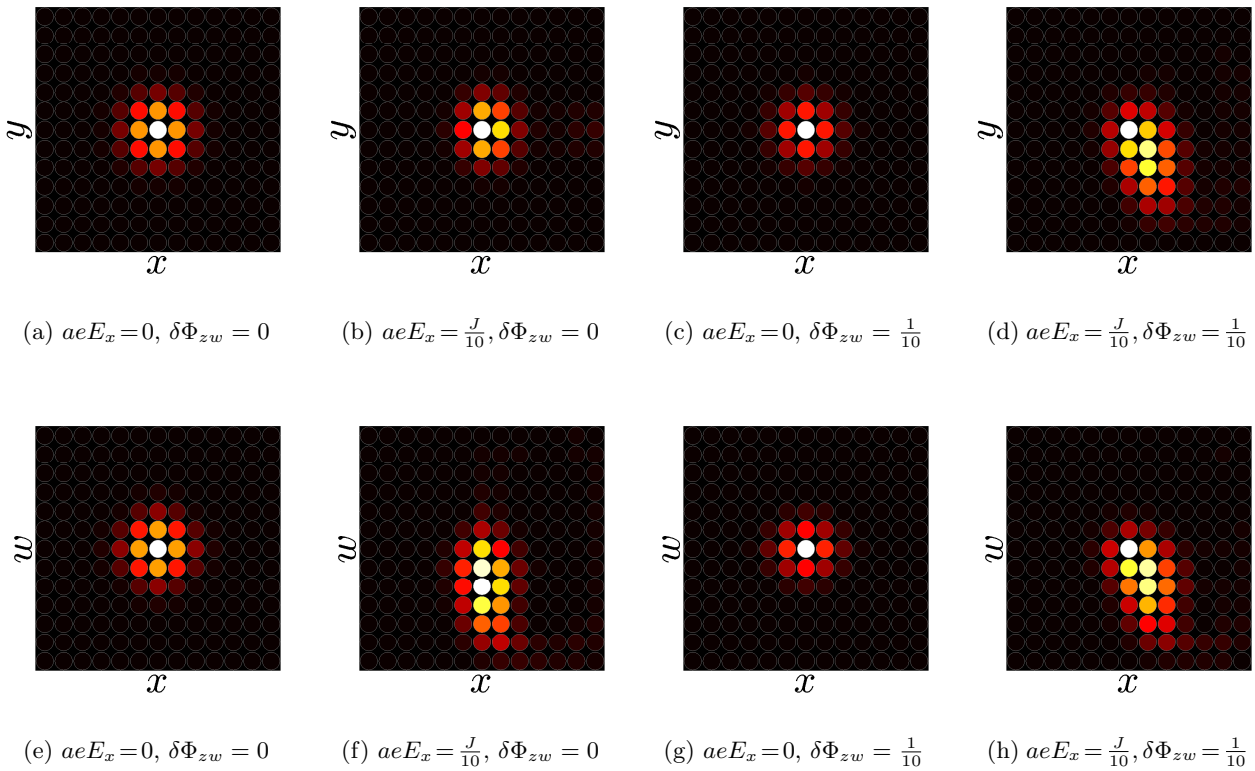

(a) $aeE_x = 0,\ \delta\Phi_{zw} = 0$ (b) $aeE_x = \frac{J}{10},\ \delta\Phi_{zw} = 0$ (c) $aeE_x = 0,\ \delta\Phi_{zw} = \frac{1}{10}$ (d) $aeE_x = \frac{J}{10},\ \delta\Phi_{zw} = \frac{1}{10}$

(e) $aeE_x = 0,\ \delta\Phi_{zw} = 0$ (f) $aeE_x = \frac{J}{10},\ \delta\Phi_{zw} = 0$ (g) $aeE_x = 0,\ \delta\Phi_{zw} = \frac{1}{10}$ (h) $aeE_x = \frac{J}{10},\ \delta\Phi_{zw} = \frac{1}{10}$

Figure 3. The optical analogue of the 4D quantum Hall effect (a)-(d) and of the 2D-like quantum Hall effect (e)-(h) in the proposed 4D photonic lattice. The numerical simulations are for a 4D lattice with 13^4 sites and with strong magnetic fields $\Phi_{xw} = 1/8$ and $\Phi_{yz} = 1/8$ and with a uniform loss rate of $\gamma = 0.03J$. The lowest energy band of this model has nontrivial Berry curvature and a second Chern number $\nu_2 = 1$. The central sites are pumped with frequency $\Omega_{\text{drive}} = -6.6J$, resonant with the lowest band. The photon steady-state is projected onto (a-d) the x-y plane and (e-h) the x-w plane for different values of perturbing fields. There is a large displacement of the photon steady-state along y only when both a perturbing electric and magnetic field are present, as expected for the response of the 4D quantum Hall effect. Conversely, there is a large displacement along w for only a perturbing electric field, as in the usual linear 2D quantum Hall effect.

from (i) a single simulation with loss-rate γ, and from (ii) a differential-measurement approach for loss-rates $\gamma_1 = \gamma + 0.005J$ and $\gamma_2 = \gamma - 0.005J$, so as to cancel out the correction $\mathcal{O}(\gamma^0)$ in Eq. (14). We observe that the differential-measurement approach improves the extracted Chern number compared to that from a single simulation provided that the loss-rate is sufficiently large compared to the energy band-width $\Delta\mathcal{E}_{\text{band}}$ that the probe beam excites all eigenstates within a band equally.

At high loss-rates, we also observe deviations from the expected Chern number as the inequality $\gamma < \Delta\mathcal{E}_{\text{gap}}$ is less well-satisfied, and eigenstates from higher bands are excited by the probe beam. The importance of ensuring $\gamma < \Delta\mathcal{E}_{\text{gap}}$ is emphasised by comparing models (A) and (B) in Figure 4. As $\Delta\mathcal{E}_{\text{gap}}(A) = 1.26J \gg \Delta\mathcal{E}_{\text{gap}}(B) = 0.28J$, we observe that a reasonable estimate of the second Chern number can be obtained up to a much larger value of γ for model (A) than for model (B). The hierarchy of energy scales $\Delta\mathcal{E}_{\text{band}} < \gamma < \Delta\mathcal{E}_{\text{gap}}$ is therefore important to take into account when designing experiments. We also note that while we have focused here on the effects of the loss-rate γ, the extraction of an accurate second Chern number can also be improved by further reducing the perturbing fields, as we have previously discussed.[1] Finally, all our numerical simulations were performed for a relatively small lattice of 13^4 sites. While this reduces the experimental requirements, this can lead to finite-size errors for the larger Chern number bands, where, as indicated by Eq. (14), the photon displacement is larger.

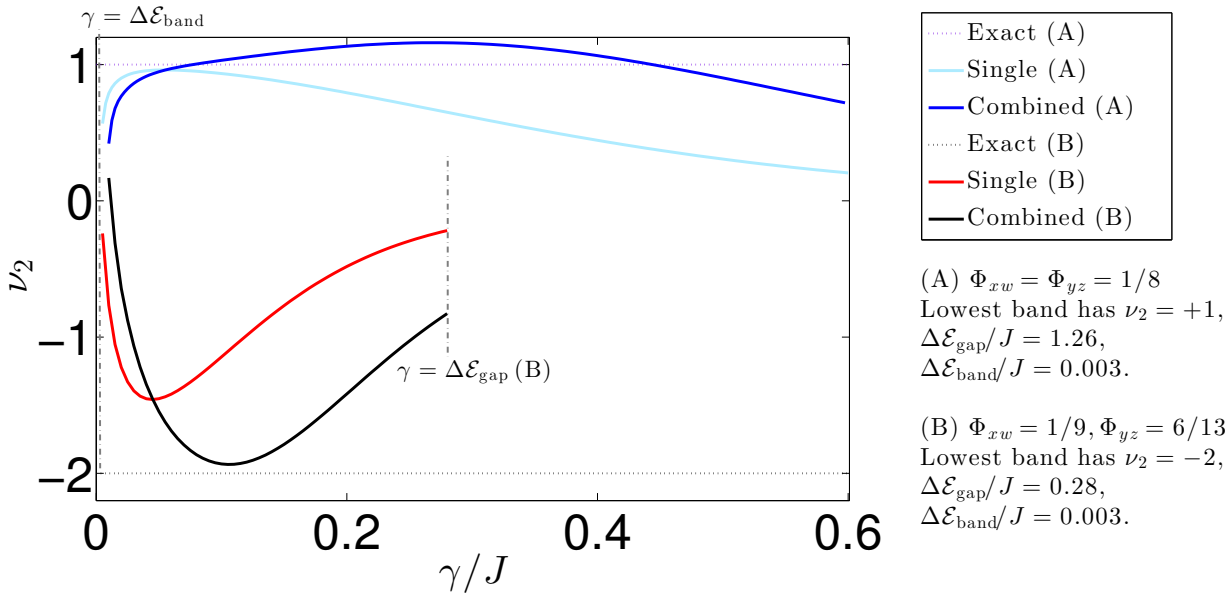

Figure 4. The extracted topological second Chern number, ν_2, as a function of the loss-rate γ for two choices of the strong fluxes. For both choices, the second Chern number is extracted (i) from a numerical simulation at loss-rate γ (denoted "Single" in the figure legend), and (ii) through a differential-measurement approach for loss-rates $\gamma_1 = \gamma + 0.005J$ and $\gamma_2 = \gamma - 0.005J$ (denoted "Combined" in the legend). With this differential approach, we can cancel out the correction $\mathcal{O}(\gamma^0)$ in Eq. (14), leading to a better estimate of the second Chern number for sufficiently high losses. At high and low loss-rates, both approaches deviate significantly from the expected second Chern number, as the inequality $\Delta\mathcal{E}_{\rm band} < \gamma < \Delta\mathcal{E}_{\rm gap}$ is less well-satisfied. Note that for model (B), we only show results up to $\gamma/J = 0.28$ where the losses become equal to the lowest band-gap. These numerical simulations were performed for 4D lattices with 13^4 sites, with a driving frequency resonant with the middle of the lowest band and with weak perturbations $aeE_x = J/100$ and $\delta\Phi_{zw} = 1/100$.

5. CONCLUSIONS

The introduction of a synthetic dimension can be an important step towards realising higher-dimensional topological lattices in integrated photonics. As we recently proposed[1] and have discussed here in greater detail, an exciting application of this approach would be to observe the 4D quantum Hall effect in the laboratory for the first time. Going further, it would be very interesting to understand the role of photon-photon interactions in a 3D system with a synthetic dimension, to see if higher-dimensional fractional quantum Hall physics could be realised. It would also be of great interest to explore the edge physics associated with this 4D quantum Hall effect, and whether there exist robust modes propagating around the 3D surface of a 4D boundary as such modes could have useful future applications in on-chip optical components.

ACKNOWLEDGMENTS

H.M.P., T.O. and I.C. are supported by the ERC through the QGBE grant, by the EU-FET Proactive grant AQuS, Project No. 640800, and by the Autonomous Province of Trento, partially through the project On silicon chip quantum optics for quantum computing and secure communications (SiQuro). H.M.P was also supported by the EC through the H2020 Marie Sklodowska-Curie Action, Individual Fellowship Grant No: 656093 SynOptic. O.Z. acknowledges the Swiss National Foundation for financial support. N.G. is financed by the FRS-FNRS Belgium and by the BSPO under PAI Project No. P7/18 DYGEST.

REFERENCES

[1] Ozawa, T., Price, H. M., Goldman, N., Zilberberg, O., and Carusotto, I., "Synthetic dimensions in integrated photonics: From optical isolation to 4D quantum Hall physics," *ArXiv e-prints* , 1510.03910 (2015).

[2] Thouless, D. J., Kohmoto, M., Nightingale, M. P., and den Nijs, M., "Quantized Hall conductance in a two-dimensional periodic potential," *Phys. Rev. Lett.* **49**(6), 405–408 (1982).
[3] Hasan, M. Z. and Kane, C. L., "*Colloquium* : Topological insulators," *Rev. Mod. Phys.* **82**, 3045–3067 (2010).
[4] Qi, X.-L. and Zhang, S.-C., "Topological insulators and superconductors," *Rev. Mod. Phys.* **83**, 1057–1110 (2011).
[5] Goldman, N., Juzeliūnas, G., Öhberg, P., and Spielman, I., "Light-induced gauge fields for ultracold atoms," *Reports on Progress in Physics* **77**(12), 126401 (2014).
[6] Jotzu, G., Messer, M., Desbuquois, R., Lebrat, M., Uehlinger, T., Greif, D., and Esslinger, T., "Experimental realization of the topological haldane model with ultracold fermions," *Nature* **515**(7526), 237–240 (2014).
[7] Aidelsburger, M., Lohse, M., Schweizer, C., Atala, M., Barreiro, J. T., Nascimbene, S., Cooper, N., Bloch, I., and Goldman, N., "Measuring the chern number of hofstadter bands with ultracold bosonic atoms," *Nature Physics* **11**(2), 162–166 (2015).
[8] Kane, C. and Lubensky, T., "Topological boundary modes in isostatic lattices," *Nature Physics* **10**(1), 39–45 (2014).
[9] Ssstrunk, R. and Huber, S. D., "Observation of phononic helical edge states in a mechanical topological insulator," *Science* **349**(6243), 47–50 (2015).
[10] Peano, V., Brendel, C., Schmidt, M., and Marquardt, F., "Topological phases of sound and light," *Phys. Rev. X* **5**, 031011 (2015).
[11] Lu, L., Joannopoulos, J. D., and Soljačić, M., "Topological photonics," *Nature Photonics* **8**, 821829 (2014).
[12] Haldane, F. and Raghu, S., "Possible realization of directional optical waveguides in photonic crystals with broken time-reversal symmetry," *Physical review letters* **100**(1), 013904 (2008).
[13] Wang, Z., Chong, Y., Joannopoulos, J. D., and Soljačić, M., "Observation of unidirectional backscattering-immune topological electromagnetic states," *Nature* **461**(7265), 772–775 (2009).
[14] Hafezi, M., Mittal, S., Fan, J., Migdall, A., and Taylor, J. M., "Imaging topological edge states in silicon photonics," *Nature Photonics* **7**, 1001–1005 (2013).
[15] Kraus, Y. E., Lahini, Y., Ringel, Z., Verbin, M., and Zilberberg, O., "Topological states and adiabatic pumping in quasicrystals," *Physical review letters* **109**(10), 106402 (2012).
[16] Rechtsman, M. C. et al., "Photonic Floquet topological insulators," *Nature* **496**(7444), 196–200 (2013).
[17] Fang, K., Yu, Z., and Fan, S., "Realizing effective magnetic field for photons by controlling the phase of dynamic modulation," *Nature Photonics* **6**(11), 782–787 (2012).
[18] Schmidt, M., Kessler, S., Peano, V., Painter, O., and Marquardt, F., "Optomechanical creation of magnetic fields for photons on a lattice," *Optica* **2**(7), 635–641 (2015).
[19] Luo, X.-W., Zhou, X., Li, C.-F., Xu, J.-S., Guo, G.-C., and Zhou, Z.-W., "Quantum simulation of 2d topological physics in a 1d array of optical cavities," *Nature communications* **6**(7704) (2015).
[20] Slobozhanyuk, A. P., Khanikaev, A. B., Filonov, D. S., Smirnova, D. A., Miroshnichenko, A. E., and Kivshar, Y. S., "Observation of topological edge modes in bianisotropic metamaterials," *ArXiv e-prints* , 1507.05158 (2015).
[21] Hafezi, M., Demler, E. A., Lukin, M. D., and Taylor, J. M., "Robust optical delay lines with topological protection," *Nature Physics* **7**(11), 907–912 (2011).
[22] Boada, O., Celi, A., Latorre, J., and Lewenstein, M., "Quantum simulation of an extra dimension," *Physical review letters* **108**(13), 133001 (2012).
[23] Celi, A., Massignan, P., Ruseckas, J., Goldman, N., Spielman, I. B., Juzeliūnas, G., and Lewenstein, M., "Synthetic gauge fields in synthetic dimensions," *Phys. Rev. Lett.* **112**, 043001 (2014).
[24] Mancini, M., Pagano, G., Cappellini, G., Livi, L., Rider, M., Catani, J., Sias, C., Zoller, P., Inguscio, M., Dalmonte, M., and Fallani, L., "Observation of chiral edge states with neutral fermions in synthetic hall ribbons," *Science* **349**(6255), 1510–1513 (2015).
[25] Stuhl, B. K., Lu, H.-I., Aycock, L. M., Genkina, D., and Spielman, I. B., "Visualizing edge states with an atomic bose gas in the quantum hall regime," *Science* **349**(6255), 1514–1518 (2015).
[26] Yuan, L., Shi, Y., and Fan, S., "Photonic gauge potential in a system with a synthetic frequency dimension," *ArXiv e-prints* , 1511.04612 (2015).

[27] Zhang, S.-C. and Hu, J., "A four-dimensional generalization of the quantum hall effect," *Science* **294**(5543), 823–828 (2001).

[28] Qi, X.-L., Hughes, T. L., and Zhang, S.-C., "Topological field theory of time-reversal invariant insulators," *Physical Review B* **78**(19), 195424 (2008).

[29] Price, H. M., Zilberberg, O., Ozawa, T., Carusotto, I., and Goldman, N., "Four-dimensional quantum hall effect with ultracold atoms," *Phys. Rev. Lett.* **115**, 195303 (2015).

[30] Bogaerts, W., De Heyn, P., Van Vaerenbergh, T., De Vos, K., Kumar Selvaraja, S., Claes, T., Dumon, P., Bienstman, P., Van Thourhout, D., and Baets, R., "Silicon microring resonators," *Laser & Photonics Reviews* **6**(1), 47–73 (2012).

[31] Estep, N. A., Sounas, D. L., Soric, J., and Alù, A., "Magnetic-free non-reciprocity and isolation based on parametrically modulated coupled-resonator loops," *Nature Physics* **10**(12), 923–927 (2014).

[32] Kraus, Y. E., Ringel, Z., and Zilberberg, O., "Four-dimensional quantum hall effect in a two-dimensional quasicrystal," *Physical review letters* **111**(22), 226401 (2013).

[33] Hofstadter, D. R., "Energy levels and wave functions of Bloch electrons in rational and irrational magnetic fields," *Phys. Rev. B* **14**, 2239–2249 (1976).

[34] Price, H. M., Zilberberg, O., Ozawa, T., Carusotto, I., and Goldman, N. *in preparation* .

[35] Ozawa, T. and Carusotto, I., "Anomalous and quantum hall effects in lossy photonic lattices," *Phys. Rev. Lett.* **112**, 133902 (2014).